The shockwise derivatives df/ds constitute partial derivatives in a local (s, n) curvilinear axis system composed of the shock wave and a straight line normal thereto through the local point of interest. Application of the equations of motion in this local system produces partial derivatives in the n direction. Vectorial considerations determine the transformation of the s derivatives and n derivatives into Y derivatives, which are the radially directed gradients sought. Details concerning the vectorial transformations are presented in Ref. 4.

In the preceding discussion, the line of interest has been the shock wave. Once the shock-wave point locations have been established, other lines composed of points located on rays at specified fractions of the distance between shock wave and reference circle are likewise established. The treatment of these lines is identical to that of the shock wave, except that the properties along the line come from the forward marching process initiated at the shock wave.

It is noteworthy that, although these intermediate grid lines may not generally be expressed as simple analytic functions, such expressions are not required for the application of the equations of motion. All that is needed is the local properties and geometric coordinates at points spaced equally with respect to a geometric spacing parameter. The difference formulas and the principles of coordinate transformation provide the necessary geometric operations. The procedures followed do not depend upon the form of the grid line.

Advancing this concept one step further, it is clear that the shock wave itself need not be a simple analytic expression. To maintain the necessary smoothness the shock wave should be analytically determined, but many analytic combinations can be devised to provide a great variety of shock shapes. In Ref. 4, examples are given for shock shapes defined simply by conic sections and then adjusted by adding radially (in the R direction) a term $a\phi^k$, where k is an even integer for axial symmetry. Such adjustments were found useful in more closely matching body contours and in extending body coverage out to local Mach numbers high enough for method of characteristics operations without resorting to extrapolation.

The idea of shock-shape adjustment has been carried even further. In an effort to very closely reproduce a body contour of interest, a series of adjustment terms has been studied. The form is

$$\Delta R = a\phi^2 + b\phi^4 + c\phi^6 + \ldots \quad (3)$$

The coefficients a, b, c, etc. were determined by an inverse matrix procedure utilizing deviations of program-produced body contours from the desired body contour as determined from cases applying selected values of a, b, c, etc., separately. Although some success was attained with this generalization, the higher accuracy required for the matrix operations often was found to approach or exceed the 8-digit accuracy supplied by the IBM 7094 in single precision operations. Further explanations and results of this extension appear in Ref. 4.

Discussion

Examples of body contour accuracies attainable from shock shape generalization are presented in Ref. 4. A useful accuracy criterion is the root-mean-square deviation $\bar{d}$ of the program-produced body contour from its sought-for exact counterpart, scaled and fitted to the program-produced body points by the method of least squares. Using a reference circle radius of 1.0, nearly spherical bodies of radii in the neighborhood of 0.75 are produced at flight Mach numbers of 6 and above. For such cases, deviations d computed along reference circle rays for optimum (i.e., minimizing $\bar{d}$) conic section shock shapes at Mach numbers of 6, 10, and 10^4 were 0.000157, 0.000130, and 0.000161, respectively. Corresponding $\bar{d}$ values obtained from shock shapes defined by a circle modified by ΔR values of $a\phi^4$, with a optimized, were improved to 0.000068, 0.000034, and 0.000017, respectively. All of the cases quoted produced reliable body coverage (data points) out to local Mach numbers somewhat beyond 1.1. Even greater improvements are attainable through shock-shape generalizations beyond the $a\phi^4$ type. Indeed, in the case of the reference circle method, shock-shape generalization beyond conic sections alone has been found an indispensable tool in defining flow fields around spherical bodies at low flight Mach numbers and around circular two-dimensional bodies. Recently, some highly accurate results were obtained for very blunt ellipsoid bodies (with body bluntness parameters B up to 4).

In summary, many varied shock-wave shapes have been generated to initiate one version of the inverse approach to the flow around a blunt body. It appears that similar geometric generalization techniques can also be applied to broaden the scope of other versions of the inverse approach.

References

[1] Van Dyke, M. D. and Gordon, H. D., "Supersonic flow past a family of blunt axisymmetric bodies," NASA TR R-1 (1959).

[2] Fuller, F. B., "Numerical solutions for supersonic flow of an ideal gas around blunt two-dimensional bodies," NASA TN D-791 (July 1961).

[3] Inouye, M. and Lomax, H., "Comparison of experimental and numerical results for the flow of a perfect gas about blunt-nosed bodies," NASA TN D-1426 (September 1962).

[4] Batchelder, R. A., "An inverse method for inviscid ideal gas flow fields behind analytic shock shapes," Douglas Rept. SM-42588 (July 1963).

[5] Milne, W. E., *Numerical Calculus* (Princeton University Press, Princeton, N. J., 1949), pp. 97, 98.

[6] Hayes, W. D. and Probstein, R. F., *Hypersonic Flow Theory* (Academic Press Inc., New York, 1959), p. 235.

Experimental Determination of Velocity Lag in Gas-Particle Nozzle Flows

DONALD J. CARLSON*
Aeronutronic Research Laboratories, Newport Beach, Calif.

Nomenclature

A	=	cross-sectional area of flow for particles
d	=	pathlength
n_1, n_2	=	real and imaginary parts of the complex index of refraction
$N(r)$	=	number of solid particles in size range Δr centered about radius r per unit volume of gas-particle mixture
$\tilde{N}$	=	number of solid particles of all sizes per unit volume of gas-particle mixture
p	=	pressure
$Q^{(e)}, Q^{(s)}$	=	efficiency factors for extinction and scattering (ratio of extinction or scattering cross section to the geometrical cross section)
r	=	particle radius
R	=	spectral radiancy
T	=	temperature
u	=	particle speed
v	=	gas speed
$\bar{w}$	=	average weight for particle size distribution

Received May 4, 1964; revision received November 6, 1964.

This work was sponsored by the Advanced Research Projects Agency under Contract NOw 61-0905-c. The author wishes to express his appreciation to R. A. DuPuis for his help with the experiments, and to S. R. Byron and W. C. Kuby for their helpful discussions. Also, he would like to acknowledge the contribution of R. A. Dobbins of Brown University who suggested the method of interpretation of the experimental results.

* Research Scientist, Fluid Mechanics Department. Member AIAA.

x,y = Cartesian coordinates
α = extinction
γ = extinction coefficient
ϵ = area ratio
θ = streamline angle
λ = wavelength
ρ = mass per unit volume
ϕ = particle-to-gas mass flow rate ratio
$\Phi(r)$ = particle distribution function

Subscripts

c = chamber
C = carbon
g = gas
p = particle
w = wall
x = axial location x
λ = wavelength λ
0 = unattenuated radiation incident upon the flame

Introduction

IT is well known that metallized solid propellant rockets produce a cloud of micron-size metal oxide particles comprising a significant mass fraction of the exhaust flow. The characteristics of such two-phase exhausts have been the subject of many investigations over the past several years. Primary motivations for these studies have included determination of performance losses caused by dynamic and thermal lags of the solids relative to the gas, prediction of radiant heat-transfer effects, and erosion problems due to particle impingement on nozzle walls.

The experiments to be described here provide a measure of the particle velocity lag. In essence, they consist of measuring the transmitted spectral radiant intensity of a tungsten ribbon-filament lamp passed through the exhaust of a solid propellant simulator[1] rocket engine. Such an engine simulates an actual solid propellant exhaust through the addition of solid particles to the combustion chamber gas of a liquid-fueled engine. Since the extinction of the lamp energy depends upon the solid particle concentration, and this concentration is related to particle velocity, measurement of the extinction yields information on the velocity. After brief discussion of theoretical velocity lag, the experimental measurements are presented and compared with lag and equilibrium (no lag) predictions; fairly good correlation with lag predictions is noted.

Nozzle Lag

Many different forms of the equations describing velocity and thermal lag of condensed phase particles in solid propellant rocket exhausts have been written and programed for numerical solution, but most are in reasonable agreement considering the uncertainties in details such as drag coefficients, particle radiation, and so on. The theoretical calculations used for comparison with the experimental values to be presented here were obtained from a simple formulation involving no coupling between the particles and the gas. Specifically, this means that the body force of the particles acting on the gas and the effects of viscous dissipation and heat transfer due to lagging particles were neglected in calculation of the gas flow field. The gas-particle expansion was characterized by use of an effective zero-lag isentropic exponent for the mixture as described by Hoglund.[2] Drag and heat-transfer formulations used were those presented by Carlson and Hoglund.[3] The existence of radial gas velocities were accounted for by assigning a radially dependent vector direction to the gas velocity simply by assuming that the gas velocity is parallel to the nozzle axis at the axis and parallel to the wall at the wall. That is

$$\theta_g = \theta_w(y_g/y_w) \tag{1}$$

To account for the nonaxial velocity vector component, an axisymmetric correction to the mass flow was applied to the continuity equation. Figure 1 shows a typical calculation of axial gas and particle velocity profiles for the nozzle used in the experiments.

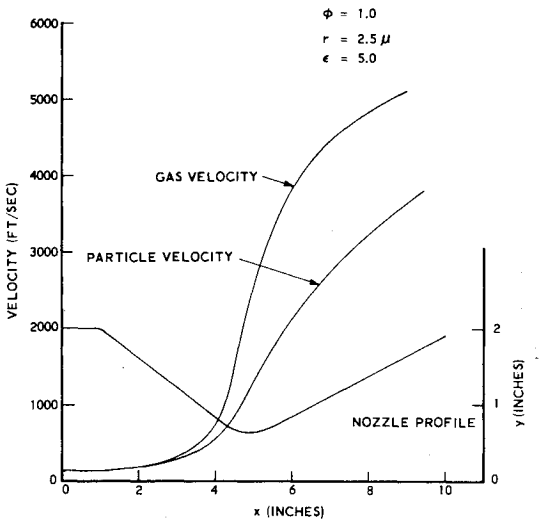

Fig. 1 Theoretical velocity profiles.

Theoretical Extinction Characteristics

A beam of light passed through an aerosol is extinguished exponentially with increasing pathlength. The rate of extinction depends upon, among other things, the concentration of particles in the beam pathlength. Since the concentration is directly related to the particle velocity, measurement of extinction will provide a measurement of velocity lag provided enough information concerning the significant parameters is known with sufficient accuracy.

The extinction of an incident beam of spectral radiancy R is expressed by

$$R = R_0 e^{-\gamma d} \tag{2}$$

where the extinction coefficient γ is a function of wavelength. For a distribution of particle sizes, we have, at a particular wavelength,

$$\gamma d = \int_0^\infty Q^{(e)}(r)N(r)\pi r^2 d(r)dr \tag{3}$$

where the pathlength d is kept inside the integral because it is desired to consider the spatial distribution of particles of various sizes. This is due to classification of sizes in the nozzle caused by slippage of particles across gas streamlines occurring when the gas turns as it passes through the De-Laval nozzle. Particles of a given size fill a cone defined by limiting streamlines† not coincident with the wall, with larger particles filling a smaller cone angle. Thus the effective pathlength for particles of a given size depends upon the cone angle and is therefore size-dependent.

Calculation of the particle concentration as a function of radial position y at axial location x is accomplished by assuming a homogeneous distribution of particles of a given size within the cone formed by their limiting streamlines. With that assumption, and using vectorial velocities calculated from the lag program, the one-dimensional continuity equation may be applied to particles of size r centered in range Δr. The continuity equation for each particle size is

$$\rho_p(r)u(r)A(r) = \text{const} \tag{4}$$

Here, $\rho_p(r)$ refers to the total mass of particles in a range Δr centered about r per unit volume of gas-particle mixture and

† The limiting streamline for a given size particle is defined as the streamline that passes closest to the nozzle wall without touching it.

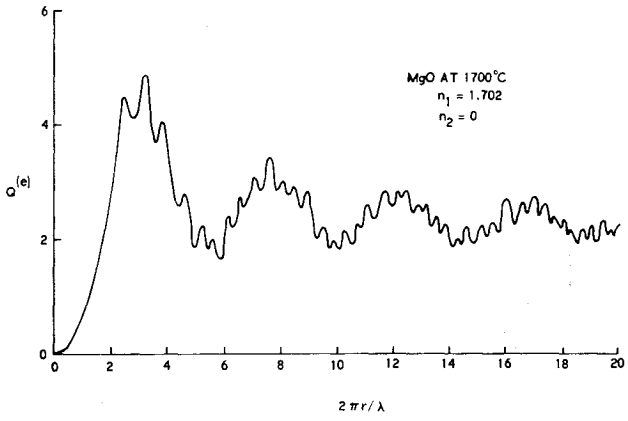

Fig. 2 Efficiency factor for extinction as a function of size parameter.

A is the cross-sectional flow area occupied by the particles in range Δr. The quantity A is a function of particle size because of the dependency of the limiting streamlines on radius. Using an average weight $\bar{w}$ (which is equal to the weight of N' particles of the distribution divided by N'), the concentration of particles in the chamber is

$$\tilde{N}_c = \frac{\rho_{p,c}}{\bar{w}} = \frac{\phi\rho_{g,c}}{\bar{w}} \tag{5}$$

In this case, $\rho_{p,c}$ refers to the total particulate mass per unit volume of gas-particle mixture in the chamber. The latter formulation may be written if $u_c = v_c$ because $\phi = \rho_p u/\rho_g v$.

The particle size distribution is characterized by a distribution function $\Phi(r)$, where

$$N(r) = \Phi(r)\tilde{N} \tag{6}$$

The continuity equation for each size particle [Eq. (4)] may be written as

$$N_c(r)u_c A_c = N_x(r)u_x(r)A_x(r) \tag{7}$$

or, since $A_c = \pi y_c^2$ and $A_x(r) = \pi d^2(r)/4$,

$$N_x(r) = N_c(r)\ [4u_c y_c^2/u_x(r)d^2(r)] \tag{8}$$

Thus, Eqs. (6–8) yield

$$N_x(r) = \Phi(r)\,\frac{\phi\rho_{g,c}u_c y_c^2}{\bar{w}u_x(r)d^2(r)} \tag{9}$$

and Eq. (3) now becomes

$$(\gamma d)_x = \frac{\phi u_c y_c^2 \rho_{g,c}}{\bar{w}} \int_0^\infty \frac{\Phi(r)Q^{(e)}(r)\pi r^2}{u_x(r)d_x(r)}\,dr \tag{10}$$

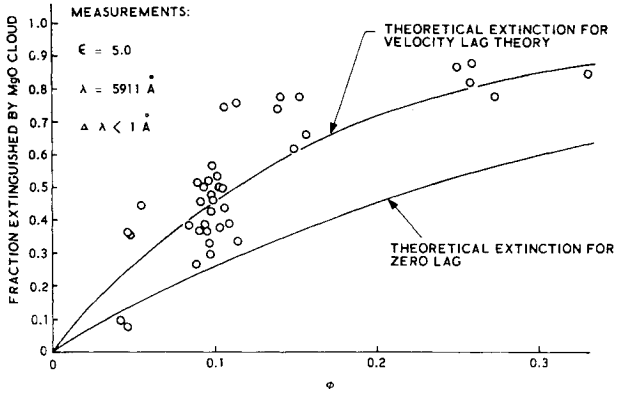

Fig. 3 Experimental and theoretical extinction for MgO cloud in rocket nozzle flow.

For the zero-lag case, particles of all sizes homogeneously fill the nozzle (assuming a homogeneous distribution at the nozzle inlet) and particle velocities become independent of particle size and equal to the gas velocity. Also, all limiting streamlines coincide with the nozzle wall. Equation (10) then becomes

$$(\gamma d)_x = \frac{\phi u_c y_c^2 \rho_{g,c}}{\bar{w}v_x d_x} \int_0^\infty \Phi(r)Q^{(e)}(r)\pi r^2 dr \tag{11}$$

The efficiency factors for extinction, scattering, and absorption by a specific material may be obtained from Mie theory[4] provided the electrical properties of the material are known at the wavelength and temperature of interest. The material used in these tests was magnesium oxide (MgO), a fairly transparent substance in the visible wavelength region. The absorption by a material is related to the imaginary part n_2 of the complex index of refraction and for transparent substances n_2 is small. For $n_2 \ll n_1$, the extinction cross section is very nearly equal to the scattering cross section, and therefore the room temperature value[5] of the real part of the index of refraction of MgO (taken at 0.58 μ wavelength) was modified for effects of high temperature (using methods outlined by Stull and Plass[6]), and calculations of $Q^{(s)}$ $(=Q^{(e)})$ were made with n_2 set equal to zero. The result is presented in Fig. 2 as a function of the size parameter $2\pi r/\lambda$.

Experimental Investigation

The experimental investigation was conducted by measuring the transmitted intensity of a beam of light passed diametrically through the nozzle of a rocket engine flowing a gas-particle mixture. This motor and the scanning grating monochromator have been described elsewhere.[7–9] Basically, the motor consists of a 1000-lb thrust engine employing gaseous oxygen to burn RP-1 fuel into which was mixed a desired amount of MgO particles of known size distribution. Essential parameters of the motor and spectroscopic instrument are tabulated in Table 1.

Table 1 Summary of rocket motor and monochromator characteristics

Chamber	
Material	copper
Coolant	water
Characteristic length	125 in.
y_c	2 in.
p_c	400 psia
Nozzle	
Convergence half angle	23°
Divergence half angle	15°
Throat radius of curvature	1.50 in.
Throat diameter	1.25 in.
Exit area ratio	7.66
Area ratio of extinction measurement	5.00
Fuels	
Fuel	RP-1 + MgO particles
Oxidizer	gaseous O_2
Fuel feed	force feed by hydraulic piston
Scanning grating monochromator	
Scan speed	2 cps
Band	5881–5911 Å
Resolution	>1 Å
Type	Jarrell-Ash Ebert grating monochromator, modified for high-resolution, rapid-scan
Detector	RCA C-70046 experimental 14 stage photomultiplier tube
Detector voltage	1800–3000 VDC

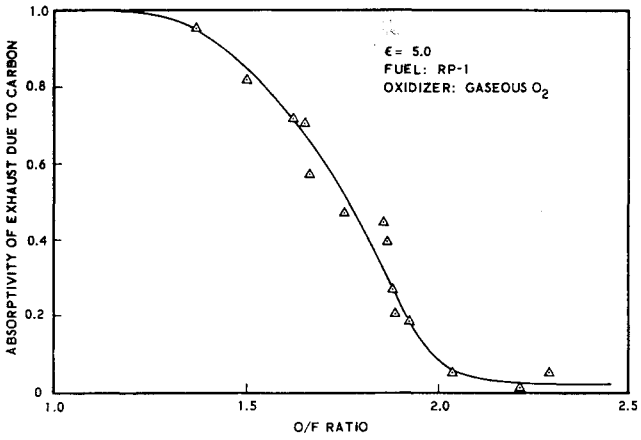

Fig. 4 Absorptivity due to solid carbon in the RP-1gaseous oxygen exhaust as a function of oxidizer-to-fuel ratio.

The transmissivity measurements were obtained through open ports located at area ratio 5, where the nozzle pressure is close to atmospheric pressure for typical tests. The transmission at 5911 Å was used here, although the spectrometer also scanned other wavelengths. A schematic diagram of the experimental system has been presented previously.[9]

The particle size distribution used in these tests was the same as that used in other experiments[7,9]; the volume to surface mean diameter is about 3 μ. The experimental data (including some extinction data points reported previously[7]) are shown in Fig. 3 compared with theoretical lag and zero lag predictions based in Eqs. (10) and (11). Although there is appreciable scatter of the data, the lag theory seems to provide a reasonable correlation.

The experimental data of Fig. 3 are not the raw data; a correction was made for extinction caused by solid carbon in the flow. This was obtained by measuring the extinction due to solid carbon for a series of tests employing RP-1 and gaseous oxygen with no oxide particles present. The results of these tests are presented in Fig. 4. The correction is made assuming the solid carbon is distributed homogeneously across the plane of measurement and using the relationship

$$1 - \alpha' = (1 - \alpha_{MgO})(1 - \alpha_C) \qquad (12)$$

where α' is the total extinction due to both carbon and MgO. It was assumed that extinction due to carbon did not change as oxide particles were added to the flow, but was dependent only on the oxidizer-to-fuel ratio.

Summary

Light extinction measurements performed in the nozzle of a rocket exhaust containing metallic oxide particles of a known size distribution have agreed with theoretical predictions based upon velocity lag theory. This establishes further evidence that such theories provide reasonable descriptions of the actual gas-particle flow processes occurring in two-phase rocket nozzle flows.

References

[1] Jones, W. H., "Solid propellant exhaust simulation," AIAA J. 1, 721–722 (1963).

[2] Hoglund, R. F., "Recent advances in gas-particle nozzle flows," ARS J. 32, 662–671 (1962).

[3] Carlson, D. J. and Hoglund, R. F., "Sphere drag and heat transfer relationships for gas-particle nozzle flows," AIAA J. 2, 1980–1984 (1964).

[4] van de Hulst, H. C., *Light Scattering by Small Particles* (John Wiley and Sons, Inc., New York, 1957), Chap. 9, pp. 114–128.

[5] Gray, D. E. (ed.), *American Institute of Physics Handbook* (McGraw-Hill Book Co., Inc., New York, 1963), 2nd ed., Chap. 6, p. 29.

[6] Stull, V. R. and Plass, G. N., "Emissivity of dispersed carbon particles," J. Opt. Soc. Am. 50, 121 (1960).

[7] Carlson, D. J., "Experimental determination of thermal lag in gas-particle nozzle flow," ARS J. 32, 1107 (1962).

[8] Carlson, D. J., "A high-resolution rapid-scan spectrometer," Aeronutronic Publ. U-2002 (January 31, 1963).

[9] Carlson, D. J., "Emittance of condensed oxides in solid propellant combustion products," Tenth Symposium (International) on Combustion, Cambridge, England, Paper 119 (August 17–21, 1964).

Step Induced Boundary-Layer Separation Phenomena

ROBERT W. HALPRIN*
Douglas Aircraft Company, Inc., Santa Monica, Calif.

Nomenclature

h = step height
P = plate pressure
P_p = plate "plateau" pressure
P_∞ = freestream pressure
δ = boundary-layer height

A NUMBER of experimental[1–3] and theoretical[4–6] studies have been conducted on the separation phenomena associated with two-dimensional steps and planar shocks interacting with a turbulent boundary layer. Much less study has been centered upon the more complicated phenomena involving a three-dimensional protuberance in a supersonic flow. In order to provide information on the effects of circumferential flow on the separated region formed upstream of a protuberance, a wind tunnel† test program was conducted utilizing two-dimensional and cylindrical steps immersed in supersonic flow. The Mach number and turbulent boundary-layer height in the test section were measured and found to be 2.71 and 0.19 in., respectively. The step heights ranged from 0.1 in. (h/δ = 0.525) to 0.5 in. (h/δ = 2.63); the cylindrical step diameters ranged from 0.5 to 1.0 in. A sketch of the test models is shown in Fig. 1.

The results of the two-dimensional step tests were found to correlate well with those of previous investigations. The pressure rise at the step face established an oblique shock wave that propagated upstream and caused the boundary layer to separate from the base plate. The length of the high-pressure region downstream of the shock wave (hereafter known as the compression region) was found to be a function of the step

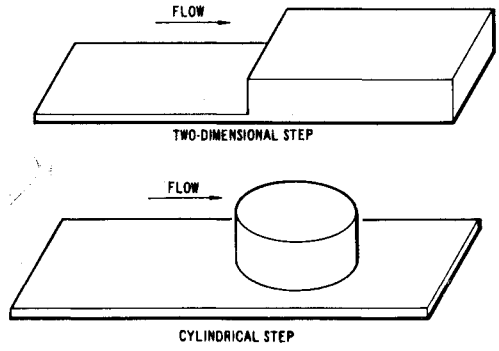

Fig. 1 Sketch of test models.

Received June 3, 1964; revision received September 14, 1964.

* Group Engineer, Missile and Space Systems Division. Member AIAA.

† The work was performed in the University of California at Los Angles supersonic wind tunnel.